Origin of the Metal-to-Insulator Transition in $H_{0.33}MoO_3$

Roger Rousseau,[†] Enric Canadell,*[,†] Pere Alemany,*[,‡] Donald H. Galván,[§] and Roald Hoffmann*[,⊥]

Institut de Ciència de Materials de Barcelona (CSIC), Campus de la UAB, 08193 Bellaterra, Spain, Departament de Química-Física, Universitat de Barcelona, Diagonal 647, 08028 Barcelona, Spain, Instituto de Física de la UNAM, Laboratorio de Ensenada, Ensenada, Baja California, Mexico, and Department of Chemistry and Materials Science Center, Cornell University, Ithaca, New York 14853-1301

Received May 8, 1997[⊗]

The electronic structure of the double octahedral layers present in $H_{0.33}MoO_3$ has been studied. It is shown that, depending on structural details, three bands, two of them having a two-dimensional character and one having a one-dimensional character, can be in competition at the bottom of the t_{2g}-block band structure. Both qualitative arguments and detailed computations show that the Fermi surface of the double octahedral layers has a two-dimensional character and does not exhibit nesting vectors. Consequently, the metal-to-insulator transition exhibited by $H_{0.33}MoO_3$ cannot be a Fermi surface driven electronic instability, as recently proposed. An order−disorder transition of the protons is suggested as a more likely origin of this resistivity anomaly.

Introduction

Hydrogen-doped molybdenum oxides of the general formula H_xMoO_3 ($0.0 < x < 2.0$) are a subclass of a much larger group of materials known as the molybdenum bronzes, some of which are low-dimensional metals exhibiting interesting phenomena such as charge density waves (CDWs), superconductivity, and nonlinear transport.[1−4] Most of these systems have extended networks of MoO_6 octahedra and a very low average d-electron count for the molybdenum atoms (i.e., between d^0 and d^1). Hence, only the lowest lying part of the t_{2g}-block levels can be filled. Distortions in some of the MoO_6 octahedra lead to short M−O bond lengths, and consequently, some or all of their t_{2g} levels are high in energy and cannot contribute in a significant way to the lowest t_{2g}-block bands. Thus, the crystal structure exerts a strong control of the topology of the bands near the Fermi level and, consequently, of their physical properties.[5]

Gentle reduction of solid MoO_3 gives rise to four distinct phases of H_xMoO_3, the structure of which is dependent upon the concentration and location of the doping atoms.[6] These compounds have a wide range of colors and crystal classes. Phase I ($0.25 < x < 0.40$) is blue in color with an orthorhombic structure, whereas phase III ($1.55 < x < 1.72$) is red with a monoclinic crystal structure. Phase II ($0.85 < x < 1.04$) and phase IV ($x = 2.0$) are blue and green respectively, both with monoclinic crystal structures. X-ray and neutron scattering experiments show that the reduction proceeds without disrupting the gross overall features of the parent orthorhombic MoO_3 lattice. Hydrogen bronzes have great technological interest due to their intense color and conductivity properties that make them suitable for applications such as electrochromic devices, fuel cells, and gas sensors. Furthermore, these materials offer a wealth of data on which relationships between solid-state structure and physical properties may be studied.

Recently, in a very thorough investigation by Adams et al.,[7] a CDW state has been reported in one of these compounds, $H_{0.33}MoO_3$. This state has been characterized by both conductivity and single-crystal X-ray diffraction measurements. $H_{0.33}MoO_3$ exhibits a metal-to-insulator transition at 380 K, which is accompanied by the observation of superstructure spots in the X-ray diffraction pattern. The supercell corresponding to these diffuse lattice spots was reported as corresponding to a tripling along the **a**-direction and a sextupling along the **c**-direction. Furthermore, the actual crystal structure of the supercell was also solved. Fröhlich conductivity as a consequence of CDW depinning was also reported. Adams et al.[7] proposed that the mechanism of the metal-to-insulator transition is a Peierls distortion caused by the nesting of a one-dimensional electronic energy band. The primary reasoning behind this assertion is that if the system were to have a conduction band that was dispersive in only the **c**-direction, the occupation of this band would be a one-sixth filling for the electron count associated with the $H_{0.33}MoO_3$, stoichiometry. Nesting of the Fermi surface associated with this one-dimensional (or pseudo-one-dimensional) band would result in a supercell with the observed sextupling.

The metal-to-metal or metal-to-insulator transitions exhibited by low-dimensional materials indeed are frequently associated with the appearance of a CDW which leads to a periodic lattice distortion and the partial or complete disappearance of the Fermi surface of the system. The necessary condition for such a CDW type instability is that the Fermi surface of the system is nested.[5,8] However, it must be recalled that not all structural modulations in metals arise because of a Fermi surface driven CDW. For instance, Mo_8O_{23}, CuV_2S_4, and 1T-$TiSe_2$ are room-

[†] CSIC.
[‡] Universitat de Barcelona.
[§] UNAM.
[⊥] Cornell University.
[⊗] Abstract published in *Advance ACS Abstracts,* September 15, 1997.

(1) Manthiram, A.; Gopalakrishnan, J. *Rev. Inorg. Chem.* **1984**, *6*, 1. Powell, A. V.; Pointon, M. J.; Dickens, P. G. *J. Solid State Chem.* **1995**, *113*, 109.
(2) *Low-Dimensional Electronic Properties of Molybdenum Bronzes and Oxides*; Schlenker, C., Ed.; Kluwer: Dordrecht, The Netherlands, 1989.
(3) Greenblatt, M. *Chem. Rev.* **1988**, *88*, 31.
(4) *Physics and Chemistry of Low-Dimensional Inorganic Conductors*; Greenblatt, M., Schlenker, C., Dumas, J., van Smaalen, S., Eds.; NATO-ASI Series B: Physics; Plenum Publ.: New York, 1996.
(5) Canadell, E.; Whangbo, M.-H. *Chem. Rev.* **1991**, *91*, 965.
(6) Birtill, J. J.; Dickens, P. G. *Mater. Res. Bull.* **1978**, *13*, 311.
(7) Adams, S.; Ehses, K.-H.; Spilker, J. *Acta Crystallogr. B* **1993**, *49*, 958.
(8) (a) Wilson, J. A.; DiSalvo, F. J.; Mahajan, S. *Adv. Phys.* **1975**, *24*, 117. (b) Pouget, J. P.; Comès, R. In *Charge Density Waves in Solids*; Gor'kov, L. P., Grüner, G., Eds.; Elsevier: Amsterdam, The Netherlands, 1989.

S0020-1669(97)00529-6 CCC: $14.00

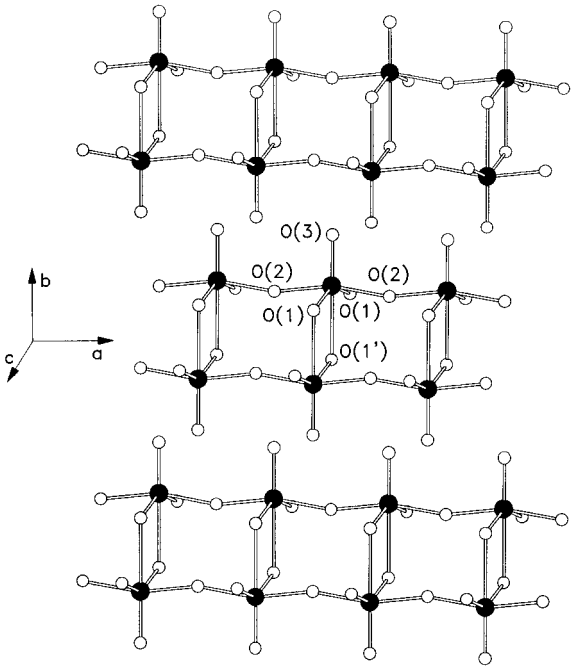

Figure 1. MoO_3 sublattice in the average structure of $H_{0.33}MoO_3$.

temperature metals exhibiting low-temperature structural modulations which have been shown to originate from other mechanisms.[9−11] Although the experimental evidence does clearly prove the existence of a structural modulation after the metal-to-insulator transition in $H_{0.33}MoO_3$, it is not altogether clear that the Peierls-type scenario is appropriate. For instance, it is not clear what role the protons play in this phase transition. The authors report that at the same temperature of the metal-to-insulator transition there is also long-range proton ordering. Hence, it is also possible that the CDW state may in fact be related to the proton ordering so that it would not be driven by a Fermi surface instability.

Previous work on molybdenum and tungsten bronzes[5] has shown that extended Hückel tight-binding band structure calculations[12] provide Fermi surfaces which are entirely consistent with experimental evidence. It has been also shown that many of the complex features of the electronic band structure and Fermi surface of these materials may be understood as arising from distortions of the MO_6 octahedra within these materials. Thus, in this paper we report an extended Hückel tight-binding study[12,13] of the correlation between the crystal and electronic structure of $H_{0.33}MoO_3$, in order to gain some understanding of the origin of its metal-to-insulator phase transition.

Crystal Structure

The MoO_3 sublattice in the average structure of $H_{0.33}MoO_3$ is shown in Figure 1. In order to discuss the origin of the metal-to-insulator transition in this phase it is essential to clearly understand the nature of the MoO_3 double layers shown there. Using the simplified representations shown in **1** they can be

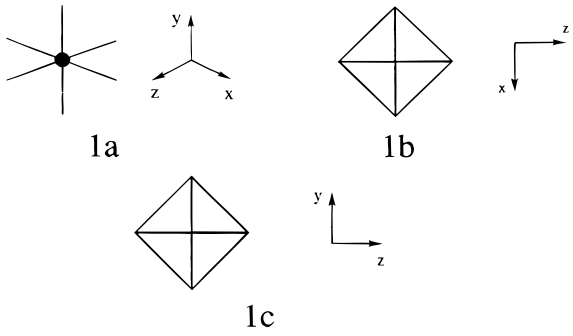

1a 1b

1c

simply described. Except otherwise stated, all along this work we will use the system of axes shown in **1** and will assume that the crystallographic **a**-, **b**-, and **c**-directions coincide with the *x*, *y*, and *z* axes, respectively. As shown in **2a**, a MoO_4 layer

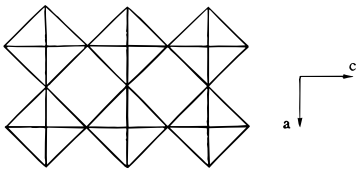

2a

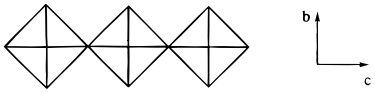

2b

can be constructed from MoO_6 octahedra by sharing the four equatorial oxygen atoms infinitely in the **a**- and **c**-directions. A side view of this layer is shown in **2b**. A MoO_3 double layer (**3**) can then be constructed from two MoO_4 layers by sharing

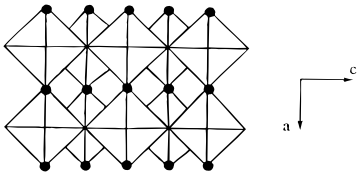

3a

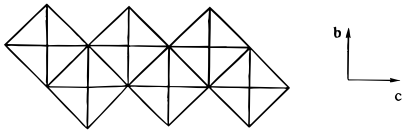

3b

two octahedral edges. Top and side views of the MoO_3 layer are shown in **3a** and **3b**, respectively. Alternatively, the MoO_3 double layer can be described as arising from MoO_4 zigzag edge-sharing octahedral chains (**4**) by corner sharing along the

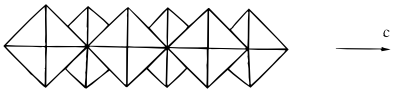

4

a-direction (see **3**). The first description emphasizes the role of the octahedral MoO_4 layers, whereas the second emphasizes

(9) Canadell, E.; Whangbo, M.-H. *Inorg. Chem.* **1990**, *29*, 2256.
(10) Whangbo, M.-H.; Seo, D.-K.; Canadell, E. In ref 4, p 287.
(11) Whangbo, M.-H.; Canadell, E. *J. Am. Chem. Soc.* **1992**, *114*, 9587.
(12) Whangbo, M.-H.; Hoffmann, R. *J. Am. Chem. Soc.* **1978**, *100*, 6093.
(13) A modified Wolfsberg−Helmholz formula (Ammeter, J. H.; Bürgi, H.-B.; Thibeault, J.; Hoffmann, R. *J. Am. Chem. Soc.* **1978**, *100*, 3686) was used to evaluate the off-diagonal $H_{\mu\nu}$ values. The atomic parameters and orbital exponents used in our calculations were taken from: Whangbo, M.-H.; Schneemeyer, L. F. *Inorg. Chem.* **1986**, *25*, 2425.

the role of the MoO_4 chains along the **c**-direction. That one or the other of these descriptions is more appropriate is going to be determined by the nature of the octahedral distortions and is the key issue of the present work.

To date there have been two powder neutron diffraction studies of the phase $H_{0.34}MoO_3$,[14,15] a single-crystal X-ray structure for the related compound $H_{0.25}MoO_3$,[16] and the superstructure reported by Adams et al.[7] for $H_{0.33}MoO_3$. In all cases, the layered structure of the parent MoO_3 phase is more or less conserved. The main structural difference concerns the way in which the MoO_6 octahedra are distorted. For instance, they are severely distorted in MoO_3, where the octahedra can be described in terms of a tetrahedral model with two oxygen atoms farther away than the four remaining ones (i.e., a 4+2 type coordination).[17] In $H_{0.33}MoO_3$, the MoO_6 octahedra adopt a more regular 5+1 type coordination. The main bond length and angles of the only symmetry-nonequivalent octahedra of the average structure are schematically shown in **5**. The

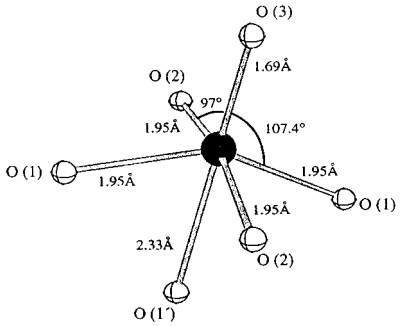

5

geometrical parameters and nomenclature, which will be those used in the subsequent discussion, are those of ref 15. These octahedra are characterized by an axial distortion (in the crystallographic **b**-direction of the crystal) such that the Mo−O(3) bond length is shorter (1.69 Å) than the average of the Mo−O bond lengths (1.97 Å) whereas the M−O(1′) is longer (2.33 Å). Such trans bond length alternation also occurs in several molybdenum oxides and bronzes and exerts a strong influence on their physical properties.[5] In addition, the O−Mo−O angles are different from 90°. Most notable are the values of 97 and 107° for the O(3)−Mo−O(2) and O(3)−Mo−O(1) angles, respectively.

The unit cell of $H_{0.33}MoO_3$ contains two double octahedral slabs stacked in the crystallographic **b**-direction. In principle, the protons can occupy both interlayer positions within the van der Waals gap and intralayer positions. The intralayer positions are those within the channels inside the slabs along the zigzag "chains" of O(2) atoms (see Figure 1 and **3a** where these O(2) atoms are indicated as black dots). Neutron diffraction,[14,15] NMR,[18] and optical spectroscopy[19] studies for H_xMoO_3 ($x \approx 1/3$) all indicate that the hydrogen atoms lie in the above mentioned intralayer positions. According to Adams et al.,[7] the superstructure found after the metal-to-insulator transition of $H_{0.33}MoO_3$, consists of a sextupling along the **c**-direction and a tripling along the **a**-direction. A direct determination of the position of the protons was not possible because of the impossibility of growing homogeneous single crystals of the appropriate dimensions. The proton sites were deduced indirectly from the Mo−O bond lengths by using a bond length−bond strength empirical formula. They were suggested to be arranged in a periodically repeating sequence of groups of six protons inside two out of every three channels of the double octahedral layers.

Electronic Structure

With the usual oxidation states O^{2-} and H^+, the molybdenum atoms in $H_{0.33}MoO_3$ have a $d^{1/3}$ electron count. Since in a Peierls-type scenario the partially filled bands determine the metal-to-insulator transition, only the bottom part of the t_{2g}-block bands needs to be analyzed. In this section we will first consider how the bottom part of the t_{2g}-block bands of an ideal MoO_4 single layer **2** can be built up. Then we will consider how these t_{2g}-block bands are modified by the octahedral distortions and layer condensation, leading to the MoO_3 double layers of $H_{0.33}MoO_3$.

A. The MoO_4 Single Layer. As it has been shown for other transition metal oxides,[5,20] the band structure of these materials may be understood in a very simple way. The t_{2g} band levels of a layer obtained by corner sharing of MoO_6 octahedra are raised in energy when the p orbitals of the shared oxygens mix with the molybdenum t_{2g} orbitals. Thus, all that one needs to do in order to evaluate the qualitative band structure is to count the number of metal−oxygen antibonding interactions which arise in the crystal orbitals at different points of the Brillouin zone. The crystal orbitals arising from the *xz* orbital at the special points $\Gamma = (0, 0)$, $X = (\mathbf{a}^*/2, 0)$, $Z = (0, \mathbf{c}^*/2)$, and $M = (\mathbf{a}^*/2, \mathbf{c}^*/2)$ are shown in **6a**−**d**, respectively. The black

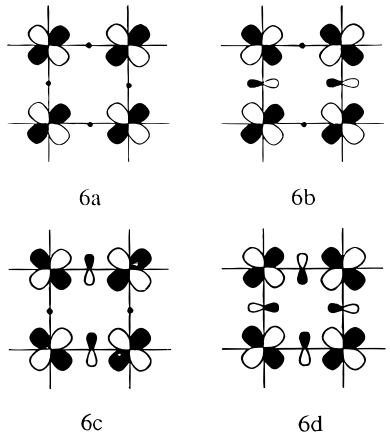

dots in these drawings represent the symmetry-conditioned absence of contribution from the bridging oxygens. Similar diagrams for the *xy* and *yz* orbitals are shown in **7a**−**d** and **8a**−**d**, respectively. For simplicity we omit the contributions from the O(1′) and O(3) positions in all diagrams. Counting how many oxygen p orbitals per unit cell mix into a given crystal orbital leads to the approximate energy of such a crystal orbital (in units of the corresponding M−O β integral). Although not shown in **6**−**8** for simplicity, to evaluate an approximate band dispersion diagram we must also take into account the axial oxygen contributions. As shown elsewhere,[5] the energy destabilization afforded by the mixing of a p oxygen orbital is approximately four times smaller when the oxygen lies in an axial position. With this relationship in mind and using diagrams **6**−**8** to count the number of Mo−O antibonding

(14) Schröder, F. A.; Weitzel, H. *Z. Anorg. Allg. Chem.* **1977**, *435*, 247.
(15) Dickens, P. G.; Birtill, J. J.; Wright, C. J. *J. Solid State Chem.* **1979,** *28*, 185.
(16) Wilhelmi, K.-A. *Acta Chem. Scand.* **1969**, *23*, 419.
(17) Kihlborg, L. *Ark. Kemi* **1963**, *21*, 357.
(18) Slade, R. C. T.; Halstead T. K.; Dickens, P. G. *J. Solid State Chem.* **1979**, *28*, 185.
(19) Eda, K. *J. Solid State Chem.* **1983**, *83*, 292.
(20) Rousseau, R.; Palacín, M. R.; Gómez-Romero, P.; Canadell, E. *Inorg. Chem.* **1996**, *35*, 1179.

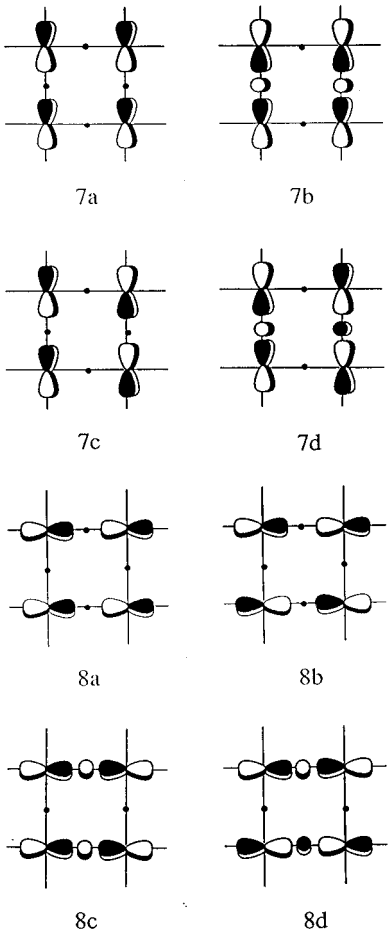

interactions (see Table 1), the qualitative band structure shown in **9** can be obtained.

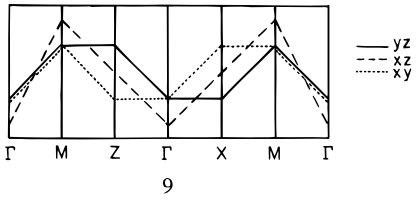

9

Several important conclusions can be drawn from **9**. First, as we are interested in the bottom portion of the t_{2g}-block bands, we note that the lowest energy crystal orbital states occur around the special point Γ and that these states are located in the *xz* band. Second, the electronic energy band derived from this orbital has significant dispersion in both directions of the layer. Third, the *xy* band is dispersive only along Γ−X (i.e., along the **a***-direction). Fourth, the *yz* band is dispersive only along Γ−Z (i.e., the **c***-direction). In conclusion, the t_{2g}-block band structure of the MoO_4 layer is the superposition of a two-dimensional (2D) band and two one-dimensional (1D) bands along the **a**- and **c**-directions. The lowest lying levels of the t_{2g}-block band are those of the 2D band. These results can however be strongly affected by the nature of the octahedral distortion and the layer condensation which we examine in the next sections.

B. Octahedral Distortion. The t_{2g} energy levels for an ideal MoO_6 octahedron with the average bond length of 1.97 Å, as well as those for the axially distorted octahedron with all O−Mo−O angles fixed at 90° and bond lengths as shown in **5**, are given in Figure 2. For comparison, we also show the same energy levels for the completely distorted octahedron, as in the actual structure of $H_{0.33}MoO_3$. The axial distortion of the octahedra causes a splitting of the energy levels leaving one of the orbitals distinctly separate from the other two orbitals. This

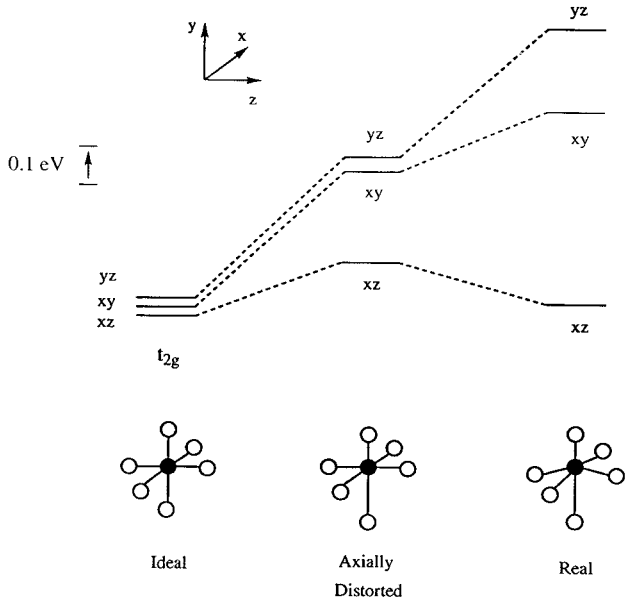

Figure 2. Energy diagram showing the three t_{2g} energy levels for (a) an MoO_6 ideal octahedron with the average Mo−O distance of 1.97 Å, (b) an MoO_6 octahedron with all angles fixed at 90° and Mo−O distances as in **5**, and (c) an MoO_6 octahedron as found in $H_{0.33}MoO_3$.

Table 1. Antibonding Contributions per Unit Cell of the Oxygen p Orbitals in the t_{2g}-Block Bands of the MoO_4 Octahedral Lattice **2**

band	crystal orbital	wave vector point	bridging contributions	axial contributions
xz	**6a**	Γ	0	0
	6b	X	1	0
	6c	Z	1	0
	6d	M	2	0
xy	**7a**	Γ	0	2
	7b	X	1	2
	7c	Z	0	2
	7d	M	1	2
yz	**8a**	Γ	0	2
	8b	X	0	2
	8c	Z	1	2
	8d	M	1	2

low-lying orbital is that which is of δ-type with respect to the direction of the bond alternation, i.e., the *xz* orbital. Angular distortion of the O−Mo−O angles further increases this separation but does not qualitatively change the diagram.

As shown in Figure 2, the *xz* orbital remains essentially unchanged in energy upon distorting the bond lengths from the average value to those exhibited in the experimental structure. Symmetry does not allow the mixing of the p-orbitals of the O(3) and O(1′) atoms into this orbital. The remaining *xy* and *yz* orbitals are directed toward the O(3) position; the shortening of the Mo−O(3) bond leads to an increased antibonding interaction and thus raises the energy levels of these orbitals. It is easy to see how this octahedral distortion is going to modify the t_{2g}-block band structure **9**: The two 1D bands will be raised in energy with respect to the 2D band. With the electron filling corresponding to Mo $d^{1/3}$, even for not very strong octahedral distortions it is clear that the partially filled levels will only be those of the 2D band.

C. Layer Condensation. Since the angular distortions only increase the energy separation between the *xz* and the (*xy*, *yz*) orbitals, let us consider the effect of layer condensation by considering a model of simple axially distorted octahedra. In Figure 3 we show a schematic molecular orbital diagram for the condensation of two MoO_6 octahedra. In the construction of this figure we neglect Mo−Mo π interactions, which should be weak for this Mo−Mo separation. We also neglect mixings in the wave functions which should be quite small due to the

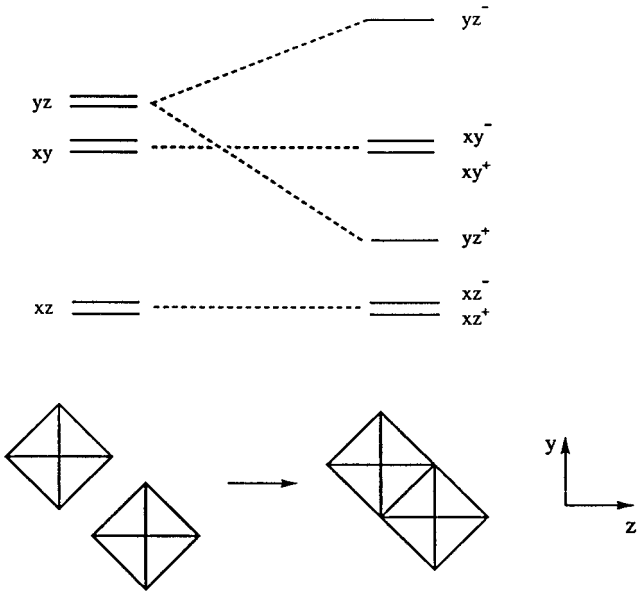

Figure 3. Schematic diagram showing the effect of octahedral edge-sharing on the t_{2g} orbitals.

local quasi-octahedral symmetry. This diagram shows that the two orbitals derived from the *xz* orbitals, here referred to as xz^+ and xz^-, respectively, remain unaffected by this condensation and provide two practically degenerate energy levels due to the orthogonality of the wave functions. Thus, the electronic energy bands which arise from these two orbitals behave essentially as the *xz* band in the MoO_4 single octahedral slab. Something similar occurs for the d_{xy} orbitals. The two new orbitals xy^+ and xy^- are again practically degenerate and may be considered as two independent *xy* orbitals. The bands which arise from these orbitals also behave as two independent *xy* bands.

The situation is completely different for the *yz* orbitals which lead to bonding (yz^+) and antibonding (yz^-) combinations. This is due to the Mo−Mo σ type interaction across the shared edge. Furthermore, the interaction with the O(1′) p orbitals is also lost in both of these orbitals. Thus the bonding yz^+ level is considerably lowered in energy. Thus, condensation can compensate for the energy raising effect of the axial distortion in the yz^+ orbital if the Mo−Mo σ interaction is strong enough. Because the *yz* orbitals lead to 1D bands which are only dispersive along Γ−Z (i.e., the **c***-direction), depending on the relative energy effect of the axial distortion and the condensation, the yz^+ orbital could well lead to the lowest t_{2g}-block band and be the partially filled band of the system.

Since we are only interested in the bottom portion of the t_{2g}-block bands, it is clear from our discussion that only the xz^+, xz^-, and yz^+ bands must be explicitly considered. The main effect of the condensation is to split the *yz* bands; the dispersion along the **a**- and **c**-directions is not affected. Thus, two of these bands (xz^+ and xz^-) are 2D whereas one (yz^+) is 1D. Consequently, it is the relative energy weight of the octahedral distortion and layer condensation which dictates what is the lowest energy band of the system and, thus, the dimensionality of the Fermi surface (i.e., 1D vs 2D).

D. Fermi Surface and Metal-to-Insulator Transition. The unit cell of the MoO_3 double layer in $H_{0.33}MoO_3$ contains two formula units. Thus, the t_{2g}-block bands are filled with only 0.66 electrons, so that $H_{0.33}MoO_3$ must possess partially filled bands. In view of the previous analysis, three different situations can be envisioned. First, the two 2D bands are the only partially filled ones. Second, the two 2D and one 1D bands are all partially filled. Third, only the 1D band is partially filled. Do we have some hint, just on the basis of the crystal structure, as

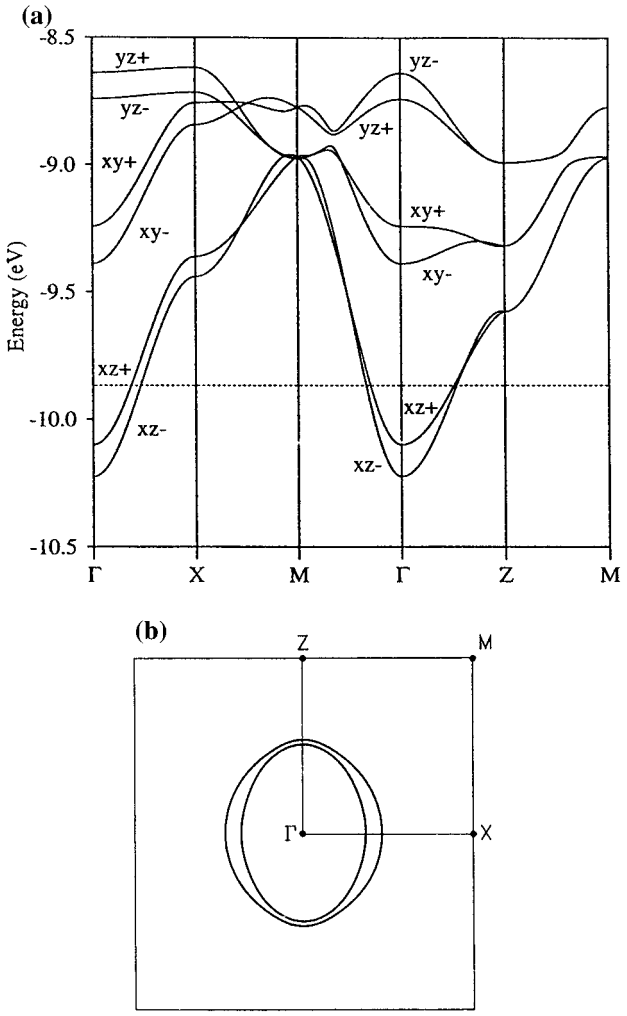

Figure 4. Calculated band structure (a) and Fermi surface (b) for the $MoO_3^{0.33-}$ double layers of $H_{0.33}MoO_3$. The dashed line in (a) indicates the Fermi level. Γ, X, Z, and M refer to the (0, 0), (**a***/2, 0), (0, **c***/2), and (**a***/2, **c***/2) wave vectors of the first Brillouin zone.

to which of the three situations should be more appropriate for $H_{0.33}MoO_3$? The first situation is favored by a strong O(3)−Mo···O(1′) bond length alternation. In fact, such bond length alternations are invariably accompanied by angular distortions such as those shown in **5**, i.e, O(3)−Mo−O(1) and O(3)−Mo−O(2) angles larger than 90°. Angular distortions such as these also favor the first situation. There are two different reasons for this. First, because they lead to an increase of the Mo−Mo distance across the shared edge. Second, because they lead to a rehybridization of the *yz* orbital (**10**) and the lobes directed

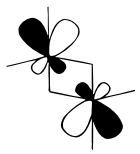

10

toward the shared edge are reduced.[20,21] As shown in **5**, the bond length alternation is quite strong and the angular distortion is such that the two angles O(3)−Mo−O(1) and O(3)−Mo−O(2) are noticeably larger than 90°. Thus, on the basis of the crystal structure alone, the first situation clearly appears as more likely.

The calculated t_{2g}-block band structure for the MoO_3 double layers in $H_{0.33}MoO_3$ is shown in Figure 4a. The important features to be noted are the following. First, the *xz* bands have

(21) Wheeler, R. A.; Whangbo, M.-H.; Hughbanks, T. R.; Hoffmann, R.; Burdett, J. K.; Albright, T. A. *J. Am. Chem. Soc.* **1986**, *108*, 2222.

2D character. Second, both the *xy* and *yz* bands have 1D character along perpendicular directions (note two avoided crossings between these two pairs of bands along $\mathbf{M} \rightarrow \Gamma$ and $\mathbf{Z} \rightarrow \mathbf{M}$ which complicate somewhat the situation). Third, the two *xz* bands are the only partially filled ones. All of these results are in excellent agreement with our qualitative model. In view of our previous discussion, the fact that the bonding−antibonding splitting of the two *yz* bands is not seen in Figure 4a is not surprising. As mentioned, the two angles O(3)−Mo−O(1) and O(3)−Mo−O(2) are considerably larger than 90° and the Mo−Mo distance is quite large (3.42 Å). Consequently, the σ type interaction between the two *yz* orbitals is almost nil. Had the angle distortion been smaller, the bonding−antibonding splitting of the two *yz* bands would have been perfectly visible. In order to check this point, we carried out a calculation for the MoO_3 double layer with exactly the same Mo−O bond lengths but all O−Mo−O angles kept at 90°. As predicted, there is a large band splitting (∼2 eV) between the two *yz* bands and the yz^+ band becomes the lowest lying t_{2g}-block band.

The calculated Fermi surface for $H_{0.33}MoO_3$ is shown in Figure 4b. It consists of two quite circular closed loops. This clearly proves that as far as the Fermi surface is concerned, the MoO_3 double layer behaves as two almost independent MoO_4 layers with bond length alternation, in perfect agreement with our qualitative analysis. This 2D Fermi surfaces show no nesting at all, and thus we are led to the conclusion that a Fermi surface instability cannot be at the origin of the metal-to-insulator transition in $H_{0.33}MoO_3$.

At this point it could be argued that this result may be an artifact of our tight-binding extended Hückel calculations. In the past, the calculated extended Hückel Fermi surfaces for low-dimensional molybdenum and tungsten oxides and bronzes have been shown to be in excellent agreement with the experimental information and have been even predictive.[5,22] Thus, there is no reason to believe that they could be seriously wrong here. In addition, it can be easily shown that our conclusion should be independent of the computational technique. Let us assume that, for some reason, the yz^+ band is really the lowest lying and only partially filled band. In that case, because of the bonding−antibonding splitting, there is just one partially filled band and, consequently, it is one-third filled. This means that the structure after the transition should exhibit a tripling along the **c**-direction and not a sextupling as experimentally observed. It can also be argued that the 1D band can be one-sixth filled if both the 1D and 2D bands are partially filled. In fact it is very unlikely that with three partially filled bands one of them will be exactly one-sixth filled. A band filling leading to an incommensurate structural modulation is much more likely. However, even if the one-sixth filling was possible for the 1D band, such sextupling can open a gap for the 1D band but not at all for the two partially filled 2D bands. Thus, in that case the sextupling along the **c**-direction will be accompanied by a metal-to-metal transition and not a metal-to-insulator transition, as experimentally found. Thus we conclude that the metal-to-insulator transition in $H_{0.33}MoO_3$ cannot be driven by a Fermi surface instability.

E. Proton Ordering and Metal-to-Insulator Transition. Since it is clear from Figure 4b that a **3a** × **6c** structural modulation cannot open a gap all over the Fermi surface, we must now speculate about a possible origin for the metal-to-insulator transition in $H_{0.33}MoO_3$. As noted before, the proton positions could not be directly located by Adams et al.[7] The modulation was found to affect mostly the O(2) (see **3a**) and Mo atoms. From a bond length−bond strength analysis[23] these authors found that the protons were located in two out of every three channels of the double octahedral layers, the third channel remaining empty. The protons were suggested to be located in periodically repeating groups of six such that, all along the zigzag "chains" of O(2) atoms, there is a periodic arrangement of "holes" and sequences of six protons. We carried out model calculations including the protons and using appropriate supercells as well as distortions of the Mo−O lattice, as found in the modulated structure. These calculations did not suggest the need for any modification in our analysis of the electronic structure of the octahedral double layers. Thus, the origin of the activated behavior of the conductivity after the transition must be found in the additional Coulomb potential brought about by the protons, which is not included in our calculations.

Since Adams et al.[7] reported that the long-range proton ordering breaks down at 380 K, i.e., at the temperature of the metal-to-insulator transition, we believe that it is the order−disorder transition of the protons which is the driving force for this transition. The strong Coulomb potential due to the protons, which reside in the channels inside the double layer (see **3a**), must have a strong effect on the conduction electrons. When the protons order at around 380 K, leading to the series of "holes" and sequences of six protons suggested by Adams et al.,[7] the conduction electrons are most likely pinned in the vicinity of such sequences of six protons. As a result, the conductivity must involve some activation energy. However, this does not mean that after the metal-to-insulator transition one out of every three Mo atoms is a Mo(V) and the rest are Mo(VI). The conduction electrons must be pinned nearby the zone where the protons are localized, but this is a relatively large zone and thus the electrons are confined into relatively large regions affecting several Mo atoms. We performed a bond length−bond strength analysis using the same formula[23] as Adams et al. and found that the transferred electrons do indeed show a wavelike pattern with a few Mo atoms being clearly Mo(VI) but most of them being in between Mo(VI) and Mo(V). Of course, the Mo atoms having greater electron densities are those adjacent to the O(2) atoms around which the sequences of six protons occur.

In conclusion, we suggest that the order−disorder transition of the protons leads to two important changes in the double octahedral layers of $H_{0.33}MoO_3$. The first of these is the pinning of the conduction electrons through the strong periodic Coulomb potential. Second, the periodic arrangement of "holes" and sequences of six protons along the zigzag chains of O(2) atoms, leads, through hydrogen bonding, to a modulation of the displacement of the O(2) atoms in the direction perpendicular to the (*ac*) plane. The propagation of such modulation to the neighboring Mo atoms leads to the modulated structure observed after the metal-to-insulator transition. Thus, we suggest that it is the order−disorder transition of protons which governs the behavior of $H_{0.33}MoO_3$ around 380 K and not a Fermi surface driven instability. The situation differs then, quite remarkably, from that in the many layered alkali-metal molybdenum bronzes which undergo metal-to-insulator transitions driven by Fermi surface instabilities.[5] Of course, the reason for such a contrasting behavior is to be found in the larger mobility of protons.

Acknowledgment. E.C. thanks Pr. C. Miravitlles for pointing out this problem. R.R. thanks the NSERC of Canada for a post graduate scholarship and Dr. S. Lee for his kind donation of computer time. P.A. acknowledges financial support from DGYCIT (Grant PB95-0848-C02-01) and CIRIT (Grant GRQ 94-1077). D.H.G. thanks CONACYT and DGAPA-UNAM for financial support.

IC9705296

(22) Whangbo, M.-H.; Canadell, E.; Foury, P.; Pouget, J.-P. *Science* **1991**, *252*, 96.

(23) Brown, I. D.; Wu, K. K. *Acta Crystallogr. B* **1976**, *32*, 1957. Bart, J. C. J.; Ragaini, V. *Inorg. Chim. Acta* **1979**, *36*, 261.